Astronomy & Astrophysics manuscript no. allende
June 20, 2014
© ESO 2014

arXiv:1406.4997v1 [astro-ph.SR] 19 Jun 2014

Deep SDSS optical spectroscopy of distant halo stars

I. Atmospheric parameters and stellar metallicity distribution.

C. Allende Prieto[1,2], E. Fernández-Alvar[1,2], K. J. Schlesinger[3], Y. S. Lee[4], H. L. Morrison[5], D. P. Schneider[6], T. C. Beers[7,8], D. Bizyaev[9], G. Ebelke[9], E. Malanushenko[9], V. Malanushenko[9], D. Oravetz[9], K. Pan[9], A. Simmons[9], J. Simmerer[10], J. Sobeck[11], and A. C. Robin[12]

[1] Instituto de Astrofísica de Canarias, Vía Láctea, 38205 La Laguna, Tenerife, Spain

[2] Universidad de La Laguna, Departamento de Astrofísica, 38206 La Laguna, Tenerife, Spain

[3] Research School of Astronomy and Astrophysics, The Australian National University, Weston, ACT 2611, Australia

[4] Department of Astronomy, New Mexico State University, Las Cruces, NM 88003, USA

[5] Department of Astronomy, Case Western Reserve University, Cleveland, OH 44106, USA
[6] Department of Astronomy and Astrophysics, The Pennsylvania State University, University Park, PA 16802, USA

[7] National Optical Astronomy Observatory, Tucson, AZ, 85719, USA

[8] JINA (Joint Institute for Nuclear Astrophysics), Michigan State University, East Lansing, MI 48824, USA
[9] Apache Point Observatory, P.O. Box 59, Sunspot, NM 88349-0059, USA

[10] Lund Observatory, Box 43, SE-221 00 Lund, Sweden

[11] Department of Astronomy, University of Virginia, Charlottesville, VA 22903, USA
[12] Institut Utinam, CNRS UMR6213, Université de Franche-Comté, Observatoire de Besan con, Besan con, France
⋆

Received April 2014; accepted June 2014

ABSTRACT

Aims. We analyze a sample of tens of thousands of spectra of halo turnoff stars, obtained with the optical spectrographs of the Sloan Digital Sky Survey (SDSS), to characterize the stellar halo population "in situ" out to a distance of a few tens of kpc from the Sun. In this paper we describe the derivation of atmospheric parameters. We also derive the overall stellar metallicity distribution based on F-type stars observed as flux calibrators for the Baryonic Oscillations Spectroscopic Survey (BOSS).
Methods. Our analysis is based on an automated method that determines the set of parameters of a model atmosphere that reproduces each observed spectrum best. We used an optimization algorithm and evaluate model fluxes by means of interpolation in a precomputed grid. In our analysis, we account for the spectrograph's varying resolution as a function of fiber and wavelength. Our results for early SDSS (pre-BOSS upgrade) data compare well with those from the SEGUE Stellar Parameter Pipeline (SSPP), except for stars with log g (cgs units) lower than 2.5.
Results. An analysis of stars in the globular cluster M13 reveals a dependence of the inferred metallicity on surface gravity for stars with $\log g < 2.5$, confirming the systematics identified in the comparison with the SSPP. We find that our metallicity estimates are significantly more precise than the SSPP results. We also find excellent agreement with several independent analyses. We show that the SDSS color criteria for selecting F-type halo turnoff stars as flux calibrators efficiently excludes stars with high metallicities, but does not significantly distort the shape of the metallicity distribution at low metallicity. We obtain a halo metallicity distribution that is narrower and more asymmetric than in previous studies. The lowest gravity stars in our sample, at tens of kpc from the Sun, indicate a shift of the metallicity distribution to lower abundances, consistent with what is expected from a dual halo system in the Milky Way.

Key words. stars: abundances, fundamental parameters, population II – Galaxy: stellar content, halo

1. Introduction

The stellar halo population in the Milky Way was first noticed among solar neighborhood stars in the previous century (Baade 1944; Chamberlain & Aller 1951), and as observational capabilities expanded, so did our knowledge about its spatial, age, metallicity, and kinematical distribution.

Dedicated surveys of the halo, such as Beers, Preston, & Shectman (1985, 1992), Norris et al. (1985), Ryan & Norris (1991), Majewski (1992), and Chiba & Beers (2000), have pioneered the sampling of halo stars at large distances. More recently, cosmological surveys of galaxies and quasars, including

⋆ Table1 is only available in electronic form at the CDS via anonymous ftp to cdsarc.u-strasbg.fr (130.79.128.5) or via http://cdsweb.u-strasbg.fr/cgi-bin/qcat?J/A+A/

observations of stars for different purposes, have taken the lead in exploring the most distant parts of the halo. The stars with the lowest known iron abundance come from candidates identified in the Hamburg-ESO survey (Wisotzki et al. 1996; Christlieb et al. 1999, 2002) or the Sloan Digital Sky Survey (SDSS; York et al. 2000, Bonifacio et al. 2012), and these studies constitute the best available database for studying the main properties of the stellar Galactic halo.

Most of the halo turnoff stars observed in the first phases of the SDSS (Stoughton et al. 2002, Abazajian 2003, 2004) were targeted as flux calibrators, with the criterion $0.1 < (g-r) < 0.4$[1], with slight variations over the years, and with additional significant numbers from SEGUE (Yanny et al. 2009), in particular their metal-poor MS turnoff and FG-type categories.

Among the four spectroscopic surveys included in the current phase of the Sloan Digital Sky Survey (SDSS-III; Eisenstein et al. 2011; Ahn et al. 2012), two are dedicated to Galactic stars. It is, however, a third program devoted to the study of the distributions of galaxy and quasar redshifts, the Baryonic Oscillations Spectroscopic Survey (BOSS; Smee et al. 2012; Dawson et al. 2013), that provides the largest samples of distant Milky Way halo turnoff stars.

In this series of papers we use the spectrophotometric calibration stars from BOSS and earlier SDSS phases to examine the main characteristics of the Galactic stellar halo. Our sample constitutes the deepest sample of halo turnoff stars and subgiants yet assembled. We describe the observations available in §2 and the analysis in §3, followed by a description of the overall halo metallicity distribution, ending with a summary in Section 5. Subsequent papers will examine variations of halo-star chemistry with distance to the center of the Milky Way in detail.

2. Observations

The spectra used in this work are included in SDSS Data Release 10 (DR10; Ahn et al. 2014) and come from the original SDSS spectrographs and their upgraded version, in operation since 2010 (Smee et al. 2012), and the 2.5-m telescope (Gunn et al. 2006) at Apache Point Observatory. They were obtained between the beginning of the survey (2000) and July 2012. Most quasars, galaxies, and stars observed spectroscopically in SDSS are chosen purely based on SDSS *ugriz* imaging (Fukugita et al. 1996; Stoughton et al. 2002; Eisenstein et al. 2011).

2.1. Instrumentation

The original SDSS spectrographs are two double spectrographs covering between 380 and 920 nm with a FWHM resolving power $\lambda/\delta\lambda$ of about 2000, fed with 640 three-arcsecond optical fibers.

The BOSS spectrographs, in operation since 2009, constitute an upgrade of the original SDSS spectrographs. The new spectrographs have a higher multiplexing ability (1000 fibers in a single exposure instead of 640), and a wavelength-dependent resolving power in the range $1300 < \lambda/\delta\lambda < 3000$ between 360 and 1040 nm. Their sensitivity is significantly enhanced from the original instruments, mainly by adopting new detectors and volume-phase holographic gratings, as well as using narrower (2 instead of 3 arcseconds in diameter) fibers that feed light from the telescope.

2.2. Target selection

We apply our analysis to the bulk of BOSS stellar spectra, which are defined as those with a measured redshift $|z| < 0.01$, or a radial velocity under 3000 km s^{-1}, obtained as of late 2011. Some of these spectra, those obtained up to July 2011, became publicly available as of July 2012 in DR9 (Ahn et al. 2012). The rest were made public in DR10 (Ahn et al. 2014). We process all BOSS spectra exactly in the same manner as the observations with the original SDSS spectrographs and they are described in §3, to derive the atmospheric parameters ($T_{\rm eff}$, $\log g$, [Fe/H]).

When available, we adopted the *Elodie* redshifts measured by the SDSS/SEGUE *spec1d* pipeline. These are obtained by template matching against a smooth version of spectra in the Elodie library (Prugniel & Soubiran 2001; Prugniel et al. 2007). When the *Elodie* redshifts were not available (*elodie_z* set to a value of zero), we embraced the standard *best* redshift values adopted by the BOSS spectral pipeline (Bolton et al. 2012).

The sample of BOSS targets with nearly zero redshift we identify is mainly comprised of

1. F-type halo turnoff stars, those used for flux calibration;
2. Cooler (mostly K and M-type) stars, selected as part of ancillary science programs or by error;
3. White dwarfs, selected either by error or associated with ancillary science programs;
4. Hybrid spectra, showing a hot source in the blue (typically a white dwarf) and a cool source (low-mass star) dominating at redder wavelengths;
5. Galaxies or (mostly) quasars, with an incorrectly assigned redshift.

Since SDSS/BOSS observations are mainly devoted to cosmology, most observations point to high Galactic latitudes, avoiding the Galactic disk and favoring the halo population. The exceptions are some of the SEGUE fields at low Galactic latitude. With an absolute magnitude $M_g \sim 5$, F-type halo turnoff stars observed by the SDSS/BOSS spectrographs are located at distances out to a few tens of kpc, and more evolved, horizontal-branch stars with similar temperatures are at distances in excess of 100 kpc.

When SDSS came into operation, the difficulty of performing flux calibration for spectra having a wide wavelength coverage over of a large area of the sky was quickly recognized. Good standards were scarce and relatively bright, a situation that, although somewhat improved, persists today. The solution adopted for SDSS was to assign spectral types and corresponding model flux distributions to the stars, scale the model distributions to match the available five-band *ugriz* SDSS photometry, and hope that the systematic errors are small and that random errors cancel out over the size of an SDSS spectroscopic plug-plate, three degrees in diameter.

F-type halo turnoff stars, in the magnitude range spectroscopically explored by the original SDSS ($14 < g < 21$), are relatively abundant and fairly easy to model, because their continua are shaped by a combination of H and H^- bound free opacity, and they exhibit limited line absorption in the optical, mainly due to iron lines. Taking BD +17 4708, with [Fe/H]= −1.7, as a prototype, the method was developed and applied, with good results. The same protocol remains in use for BOSS, using somewhat fainter stars.

[1] Here and throughout the rest of the manuscript, it is understood that the magnitudes and colors are corrected for the effects of absorption and reddening along the line of site, based on the approach of Schlegel et al. (1998).

As in earlier phases of the SDSS, halo turnoff F-type stars are identified in BOSS observations by their colors. Typically 16 of these stars are included per plugplate for flux calibration. These stars satisfy

$$\begin{aligned} 15.0 &< r < 19 \\ u-g &= 0.82 \pm 0.08 \\ g-r &= 0.30 \pm 0.08 \\ r-i &= 0.09 \pm 0.08 \\ i-z &= 0.02 \pm 0.08, \end{aligned} \quad (1)$$

with slight variations used in the early phases of the project. These stars are chosen based on the colors of the SDSS standard BD +17 4708 (Oke 1990; Fukujita et al. 1996; Bohlin & Gilliland 2004; Ramírez et al. 2006); in addition, to satisfy the color and magnitude range in the table, they are ranked in priority by their color resemblance to the standard star.

3. Analysis

Our analysis of the SDSS/BOSS spectra follows in its fundamentals the methods described by Allende Prieto et al. (2006). However, a number of improvements have been implemented. We describe the basics and updates below.

3.1. Analysis strategy and model spectra

The BOSS spectrographs have a significant variation in the resolving power as a function of wavelength. We account for such variations by using the arrays of FWHM values that accompany the spectra and, through use of a grid of model spectra with higher resolution ($\lambda/\delta\lambda = 6400$), convolving the model spectra as we fit the observations according to the FWHM for each wavelength and fiber.

The actual rest wavelengths of each BOSS spectrum differ from the others in the same plugplate as a result of the stars' radial velocities. To avoid further interpolations in the observations, we resample the model fluxes as we fit the data. BOSS and earlier SDSS spectra are preprocessed with a custom IDL pipeline that rewrites the fluxes, wavelengths and line-spread functions for each spectrum in the format appropriate for FERRE, our FORTRAN90 fitting code (Allende Prieto et al. 2006, 2009). We performed tests fitting either spectra with their spectral energy distributions (suitably normalized by a constant to make them independent of distance) or continuum normalized spectra, finding that the latter method provides better results. Best-fitting parameters and spectra and estimated errors, were stored for further study.

Our method consists of finding the optimal set of model atmosphere parameters that best matches the observed spectra. We evaluate the fitness of the models with a simple χ^2 criterion. For speed, model fluxes are precalculated on a regular grid based on classical one-dimensional Kurucz model atmospheres, and we interpolate in the three parameters under consideration ($T_{\rm eff}$, $\log g$ and [M/H]) using a quadratic Bezier scheme.

We make use of Kurucz model atmospheres (Castelli & Kurucz 2004), and the ASSET spectral synthesis code (Koesterke, Allende Prieto & Lambert 2008; Koesterke 2009). We adopt detailed continuum opacities from the compilation by Allende Prieto et al. (2003) and subsequent updates (see, e.g., Allende Prieto 2008). Line data are mainly from the calculations and literature compilations by Kurucz (available from his website[2]), enhanced with damping constants from Barklem (2007 and references therein) when available.

We calculated a grid of model spectra covering $-5 <$[Fe/H]$< +0.5$ and $0.5 < \log g < 4.5$ in steps of 0.5 dex, and $4750 < T_{\rm eff} < 6500$ K, in steps of 250 K. The α/Fe ratio adopted was solar at [Fe/H]= 0, and then linearly increasing toward lower [Fe/H], reaching +0.4 for [Fe/H]≤ -1.5, in agreement with the typical values found for stars in the Milky Way[3]. We adopted solar reference abundances as in Asplund et al. (2005), and the overall metallicity of the model atmospheres was consistent with those adopted in the spectral synthesis, with the exception of the lowest metallicities, for which no model atmospheres were readily available for our grid nodes. Model atmospheres with [Fe/H]= -2.5 were adopted for [Fe/H]= -3, and those with [Fe/H]= -4 were adopted for [Fe/H]= -5.0, -4.5, and -4.0. The grid employed included 864 model spectra: $12 \times 8 \times 9$ ([Fe/H]/$\log g/T_{\rm eff}$).

The parameters inferred from our analysis cannot be more accurate than the models used to interpret the observations. Since we rely on large numbers of precalculated synthetic spectra, we cannot consider aspects such as departures from LTE or hydrodynamical (3D) effects. Nevertheless, we expect the impact of such a simplification on the derived parameters will be quite uniform, given the limited range in temperature and metallicity of the stars we consider. As mentioned earlier, metal-poor F-type stars are one of the simplest spectral types to work with.

Despite the BOSS spectrographs offering an increased spectral range over the earlier SDSS spectrographs, we decided to adopt a wavelength region common for the two data sets. This decision was motivated by the need to evaluate the quality of our derived parameters and the availability of parameters for large numbers of SDSS stars from the SEGUE (Yanny et al. 2009) Stellar Parameter Pipeline (hereafter SSPP; Lee et al. 2008a,b; Allende Prieto 2008) and a desire to combine SDSS-I, SEGUE, and BOSS observations.

Figure 1 shows two examples of observed BOSS spectra, and our best-fitting models. At very low metallicity, the information on the stellar properties comes mainly from hydrogen (Balmer and Paschen) lines, Ca II lines (H and K in the blue, as well as the IR triplet). Our continuum correction scheme splits the spectral range into 20 equal-velocity bins and divides each by its mean value. This approach removes large-scale systematic errors in flux, preserves some of the local information on the continuum shape, and since it is a linear transformation, it is robust (symmetric) against noise. This is an unusual continuum normalization procedure, but extensive tests with simulations led us to conclude that it is very robust and performs better than other, more commonly used methods for this kind of spectra. Exactly the same procedure is applied to both models and observations.

3.2. Validation of parameters against SDSS/SEGUE

Stellar spectra taken with the SDSS spectrographs before the BOSS upgrade benefit from the added value of the SSPP. This software suite derives atmospheric parameters ([Fe/H]/$\log g/T_{\rm eff}$ and [α/Fe]) for most normal stars, and it has been continuously upgraded (Lee et al. 2011, Smolinski et al. 2011). The SSPP offers an excellent comparison to our analysis, since our techniques can be equally applied to BOSS or earlier SDSS spectra.

[2] kurucz.harvard.edu

[3] This assumption will break down for some stars. See, e.g., Cohen et al. (2013).

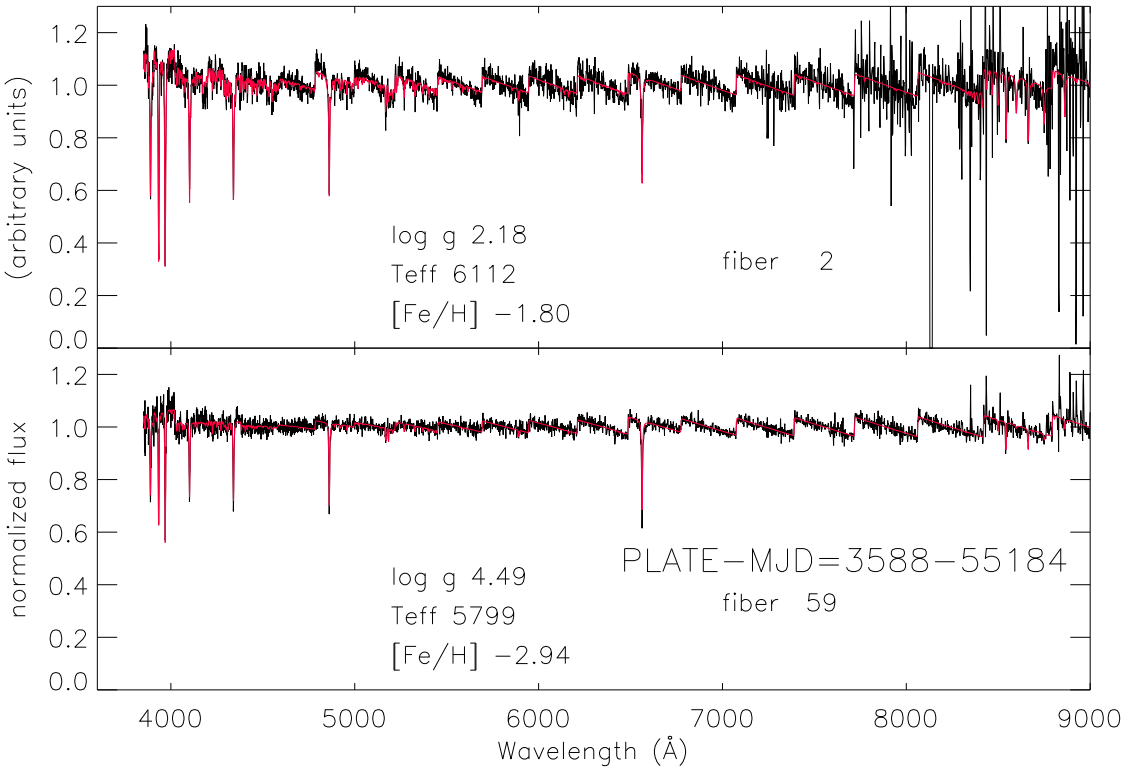

Fig. 1. Sample BOSS spectra (black) for two representative low-metallicity F-type stars, a dwarf and a giant. The spectra are divided into 20 equal-velocity bins and normalized by their mean value in each bin, as described in the text. The best-fitting parameters and models (red curves) are shown.

The SSPP includes a wide variety of techniques to derive each atmospheric parameter. The stellar effective temperature is the one that admits more variants, from Balmer-line equivalent widths, to colors, line ratios, or spectral fitting – about ten different methods are considered by the SSPP. Metallicity is also measured by a number of techniques, while gravity is the most difficult parameter to extract, and only a handful of methods are available as part of the SSPP. Only a few of the techniques derive all parameters simultaneously and in a consistent manner.

An earlier version of our fitting code is included in the SSPP. However, it is only one of many, and the version in the SSPP uses earlier grids of model fluxes, limited to a narrow spectral range (440-550 nm). The main differences between our analysis and the SSPP are:

– We use only a single method, avoiding the complex problem of combining multiple techniques with different performance levels over the parameters space;
– We use a large fraction of the spectral range available from the SDSS spectrographs;
– We account for the varying resolution of the spectra with wavelength and fiber.

We have processed all spectra in DR8 (Aihara et al. 2011) showing low redshifts ($cz < 3000$ km s^{-1}) with our method. This selection criterion identified 545 343 spectra. We further trimmed this control sample by selecting objects that we estimated to have an average signal-to-noise ratio per pixel[4] between 400 and 800 nm higher than 30. They were fit by our models with a reduced $\chi^2 < 10$, that both our method and the SSPP find to be in the range $4750 < T_{\rm eff} < 6500$ K, and with metallicities [Fe/H]< -1, in order to eliminate the bulk of the Milky Way disk system. These criteria returned a sample of 61 040 stars, for which we have compared our atmospheric parameters and those from the SSPP. The results are illustrated in Fig. 2.

The agreement between the SSPP effective temperatures and metallicities in this range of atmospheric parameters is excellent. Gaussian fittings to the distribution of the differences between this work and the SSPP are 2 ± 70 K, 0.17 ± 0.24 dex, and -0.05 ± 0.11 dex for $T_{\rm eff}$, $\log g$, and [Fe/H], respectively (see lefthand panels in Fig. 2).

The agreement is not as good for surface gravity, with our values slightly higher for dwarfs by about 0.15 dex, and significantly lower for giants ($\log g < 2.5$), with discrepancies reaching up to 1 dex at $\log g \simeq 1$. The surface gravities from the SSPP have been throughly tested against globular and open clusters (Lee et al. 2008b, Smolinski et al. 2011) for gravities as low as $\log g \simeq 1.7$, and therefore we suspect our values for low-gravity stars. Examining the stars of this sample which belong to the globular cluster M13 clearly reveals a correlation for the metallicity with gravity at $\log g < 2.5$, as illustrated in Fig. 3. Thus, the metallicity estimations for stars at this range are systematically underestimated owing to the errors in surface gravity. That leads us to be cautious with those parameters derived at $\log g < 2.5$, which will be excluded in our subsequent analyses. This effect could at least be partly related to the fact that low surface gravity red giants have temperatures that are close to our grid limit. On the other hand, the dispersion observed in our inferred metallicities for M13 stars with $\log g > 2.5$ is $\sigma = 0.06$

[4] One pixel spans 69 km s^{-1} in velocity.

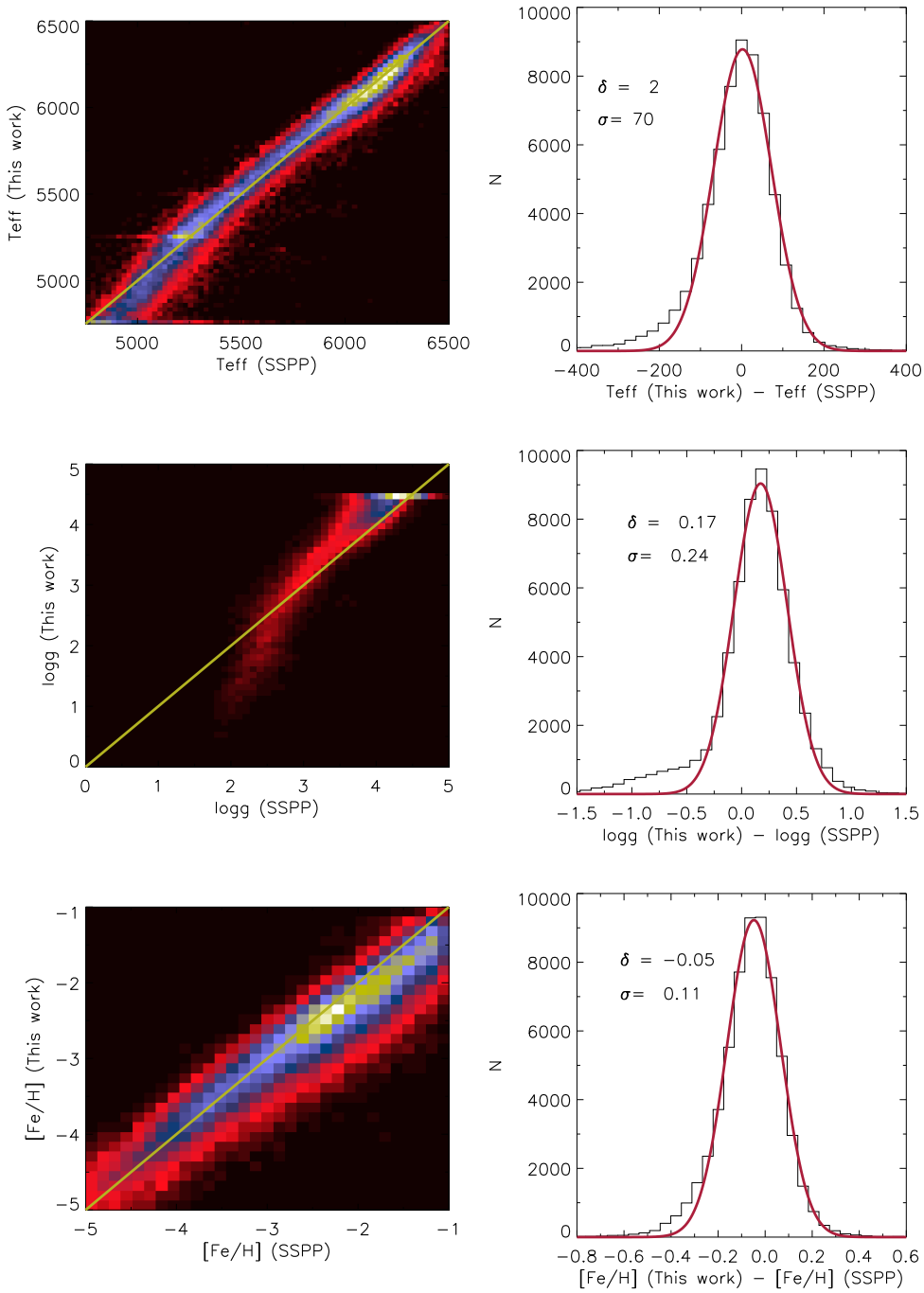

Fig. 2. Comparison between the parameters derived by our method and those from the Segue Stellar Parameter Pipeline (SSPP) for 61,040 F- and G-type stars in DR8. The lefthand panels show the density distribution of stars in a logarithmic scale, with the one-to-one relationship shown in yellow. The righthand panels show the distribution of differences between this work and the SEGUE SSPP for each parameter, with Gaussian fittings and their central values in red.

dex, significantly lower than that corresponding to both DR8 and DR9 SSPP metallicity values for the same stars, $\sigma = 0.14$ and $\sigma = 0.13$, respectively.

The model grid is limited to $\log g \leq 4.5$ due to the inclusion of very low metallicities, for which no model atmospheres for stars of higher gravity are available in the Castelli & Kurucz (2004) grids we employ. We have built grids limited to [Fe/H]≥ -2.5 that reach $\log g = 5$, but are otherwise identical, for other analyses presented in the following papers in this series.

As explained above, although BOSS spectra have a broader spectral range than the one provided by the SDSS spectra in DR8, we limit our analysis to the range 380-900 nm, common to all data. Thus, we expect that our confidence on the metallicities we derive for metal-poor stars in DR8 can be extended to stars observed by BOSS with similar properties and signal-to-noise ratios.

DR9 involved some changes in the SSPP, mainly that the effective temperatures were calibrated to match the infrared flux

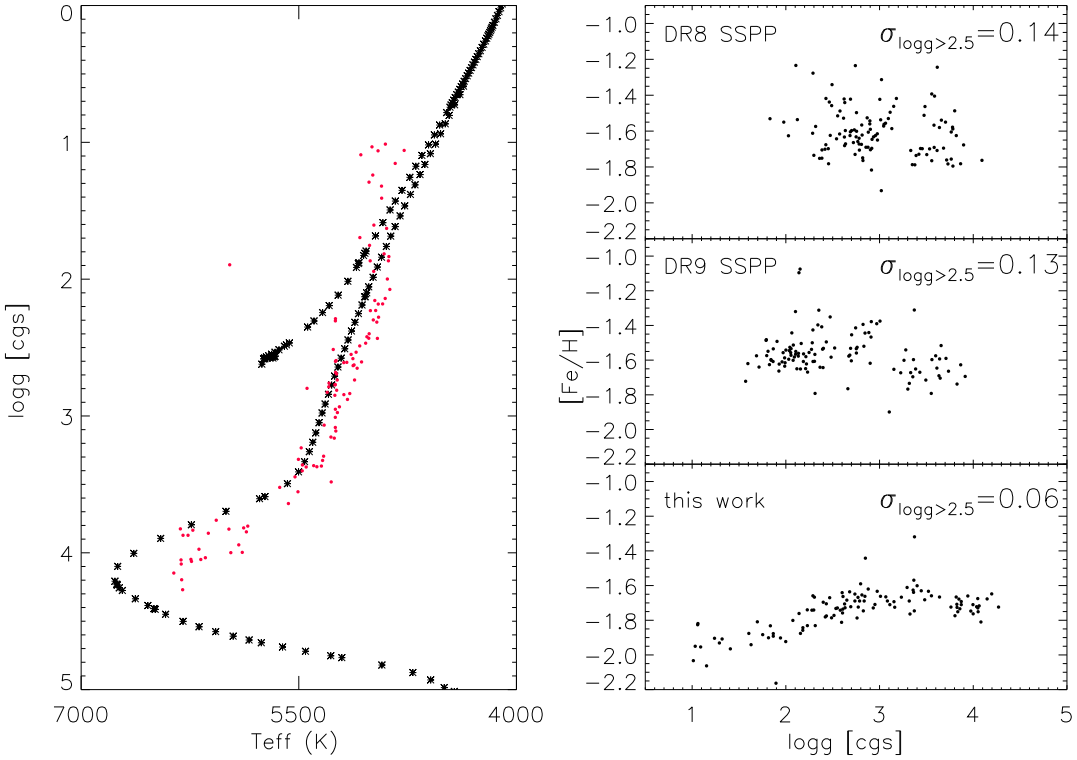

Fig. 3. Analysis of the stars belonging to the globular cluster M13. The left panel compares the stars (red dots) with an isochrone (black asterisks) at 10.0 Gy and Z=0.0004 from Girardi et al. (2002). In the right panel [Fe/H] vs $\log g$ values from the SSPP in DR8 and DR9 are plotted at the top; the bottom panel is the same plot for our results, which shows evidence of a systematic decrease in the metallicity with the surface gravity at $\log g < 2.5$ but a significant improvement in precision over the SSPP results.

method scale (see, e.g., Casagrande et al. 2010). Repeating the previous comparison but adopting the SSPP DR9 parameters we find a very similar agreement, although systematic offsets are more prominent than in DR8. The Gaussian fittings to the distribution of the differences between this work and the SSPP are -54 ± 66 K, 0.23 ± 0.23 dex, and -0.11 ± 0.11 dex for $T_{\rm eff}$, $\log g$, and [Fe/H], respectively.

3.3. Validation against individual-line analysis of BOSS spectra

A second method investigating the accuracy of the metallicities obtained in the analysis of BOSS spectra was implemented. This analysis focused on the Ca II (H and K) resonance lines (centered at about 397 and 393 nm), which saturate at high metallicity, but are a useful metallicity proxy at [Fe/H]< -1. Similar to our primary algorithm, we determine [Fe/H] by comparing the χ^2 between observations and model spectra, but this time using only wavelengths in the vicinity of the Ca II lines, confining the comparison to the $T_{\rm eff}$ and $\log g$ values previously obtained, and varying [Fe/H]. A preliminary χ^2 minimum is found by fitting three points with a parabola. We then evaluate the χ^2 at five additional values of [Fe/H] around the minimum ($\pm$0.2 dex and $\pm$0.4 dex), then fitting a new parabola to the constrained region around the minimum.

This method relies strongly on the fact that metal-poor stars have enhanced Ca/Fe ratios relative to solar proportions and will fail when this is not true, or when the enhancement is far from the assumed value (+0.4 at [Fe/H]≤ -1), but this caveat also applies to our main method. We derive an estimate of the uncertainty in the metallicity associated with the noise in the spectrum, although this ignores the error covariances with $T_{\rm eff}$ and $\log g$, since these are held constant. We tested approximately a thousand stars with metallicities between $-3 <$[Fe/H]< -1 and found excellent agreement with our main algorithm, with a mean metallicity about -0.09 dex lower, and an rms deviation of 0.11 dex. An attempt to consider both the Ca II resonance lines and the Ca II IR triplet at about 860 nm provided slightly worse results.

3.4. Additional validations

A number of recent studies from the literature have investigated metal-poor stars from SDSS. We can use these to obtain an additional constraint on the accuracy of our atmospheric parameters.

As part of a larger sample Allende Prieto et al. (2008) analyzed a homogeneous set of high-resolution spectra from HRS on the 10-m Hobby-Eberly Telescope (Tull et al. 1998) for 81 stars that had been previously observed with the SDSS spectrographs. Most of these stars have higher metallicities than those we are concerned with, but nevertheless we find good agreement between our derived parameters for the 74 stars in the sample that are cooler than 6500 K (the warmest temperature we include in our sample) and the parameters published by Allende Prieto et al. (2008). Our metallicities are on average 0.1 dex lower, our temperatures are 130 K warmer, and our gravities are 0.25 dex higher than those from the high-resolution analysis, with rms dispersions between the results of the two analyses (measured by fitting Gaussians to the residuals) of 0.18 dex, 163 K, and 0.23 dex in [Fe/H], $T_{\rm eff}$, and $\log g$, respectively.

Bonifacio et al. (2012) present high-resolution VLT/UVES (Dekker et al. 2000) observations of 16 metal-poor stars with

[Fe/H]< −3 identified from SDSS DR6 (Adelman-McCarthy et al. 2008). We have analyzed the SDSS spectra of these stars and compared our derived parameters with those from the analysis of high-resolution spectra published by Bonifacio et al. Ignoring one star (SDSS J002113-005005) that is warmer than the models in our grid ($T_{\rm eff}$ ∼ 6550 K), the agreement is excellent. Our effective temperatures are on average 63 K higher, with an rms scatter between the two sets of results of 114 K. Similarly, our gravities are, on average, 0.13 dex higher with an rms scatter of 0.46 dex, and our metallicities are 0.3 dex higher with an rms scatter of just 0.2 dex.

The same team of authors has recently announced the discovery of a dwarf star with a metallicity around [Fe/H]∼ −5, SDSS J102915+172927, originally identified as a candidate for ultra-low metallicity from the pool of SDSS spectra and later analyzed with higher resolution data from the X-shooter and UVES spectrographs, both on the VLT. Our analysis of the SDSS spectrum of this relatively *bright* star for our sample (g = 17.3) yields estimates of $T_{\rm eff}$ = 5888 K, $\log g$ = 4.47, and [Fe/H]= −4.4, which compare well with those from the high-resolution analysis by Caffau et al. (2012), namely $T_{\rm eff}$ = 5811±150 K, $\log g$ = 4.0± 0.5, and [Fe/H]= −4.89 ± 0.10.

An investigation by Yong et al. (2013), using several high-resolution spectrographs, includes results on four stars originally observed with the SDSS spectrographs. We compared our measurements for three of the stars, for which the team has derived the three atmospheric parameters; our temperatures are an average of 9 K cooler with an rms scatter of 88 K, our surface gravities are on average 0.02 dex higher with an rms scatter of 0.57 dex, and our metallicities are an average of 0.34 dex higher with an rms of 0.25 dex. For the fourth SDSS star (SDSS J014036+234458), Yong et al. derived the effective temperature and metallicity assuming that the star was either a dwarf or a giant, finding a $T_{\rm eff}$ = 5703 K and [Fe/H]= −4.0 or −4.1, respectively. Our analysis of the SDSS spectrum returned $T_{\rm eff}$ = 5958 K, [Fe/H]= −3.4, and $\log g$ = 3.8.

Aoki et al. (2013) have published atmospheric parameters and compositions for 137 stars, most of them on the turnoff, selected for having very low metallicities from SDSS/SEGUE. From 111 stars in common, we find that our $T_{\rm eff}$, $\log g$, and [Fe/H] values differ an average of −99 K (σ = 212 K), −0.01 dex (σ = 0.62 dex), and +0.13 dex (σ = 0.34 dex), respectively, from theirs. This comparison adds very little to the discussion about surface temperatures and gravities in §3.2, since these authors embrace the effective temperatures provided by the SSPP and assume a constant $\log g$ of 4.0 with an expected uncertainty of about 0.5 dex for their turnoff stars. The large scatter in $T_{\rm eff}$ is driven by a number of outliers at low temperature (T < 5000 K); a robust scatter estimate from a Gaussian model, as performed in §3.2, would instead show a mean offset of −27 K and a σ of 93 K, in fair agreement with the spread shown in the top panel in Fig. 2. Of relevance is the modest offset and scatter in metallicity, which Aoki et al. derive from Fe I lines in high-resolution Subaru/HDS spectra (Noguchi et al. 2002). This scatter is about three times larger than the overall figure of ≈ 0.1 dex in Fig. 2, at least partly because most of the Aoki sample spans the range −3.5 <[Fe/H]< −2.5; i.e., they have about one full dex lower metallicity than the median of the sample considered in Fig. 2.

Overall, all these comparisons provide high confidence in our analysis of SDSS spectra of F and early G-type metal-poor stars and, in particular, on the inferred metallicities.

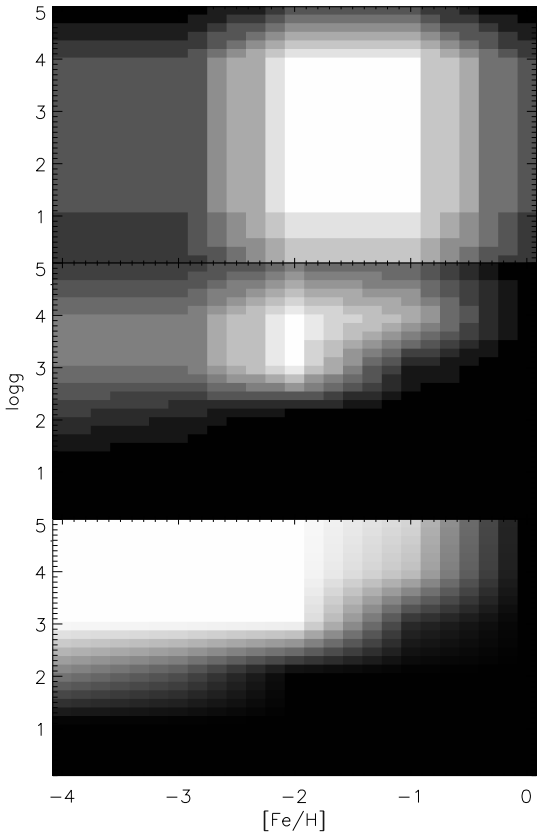

Fig. 4. Analysis of the distortions in the observed metallicity distribution due to the BOSS color cut for the selection of spectrophotometric standards. The top panel shows the distribution of models under consideration (and listed in Table 1). The middle panel shows the distribution of models that pass the color cut in Eq. 1. The bottom panel shows the ratio of the middle and top panels. White indicates higher numbers on a linear scale. See text for details.

4. The halo metallicity distribution function

For our study of halo stars we selected those targeted in BOSS as spectrophotometric standards. These are labeled as `SPECTROPHOTO_STD` by the pipeline, and they represent a homogeneously selected sample of metal-poor stars.

We limited the surface gravity to 2.5 < $\log g$ < 4, and g > 17. All else being equal, stars with lower gravities are more extended and luminous, and they probe larger distances. Using stellar evolution models, we find that the above magnitude and gravity limits place our sample at distances beyond 5 kpc, restricting it mainly to a halo population. We further limited our sample to stars fit with a χ^2 < 3 and a $T_{\rm eff}$ > 5600 K. For our selection of BOSS plugplates, this sample comprises about 5100 stars. If we instead consider a more relaxed upper limit in surface gravity, 2.5 < $\log g$ < 4.4, our sample includes about 16 000 stars. We checked that imposing an additional selection on the average signal-to-noise ratio per pixel to be higher than 30 did not alter our results significantly. Repeated observations are about 12%, and therefore their effect on our analysis is negligible, but they provide a consistency check. We find a mean rms for matched pairs of 73 K, 0.29 dex, and 0.16 dex in $T_{\rm eff}$, $\log g$, and [Fe/H], respectively.

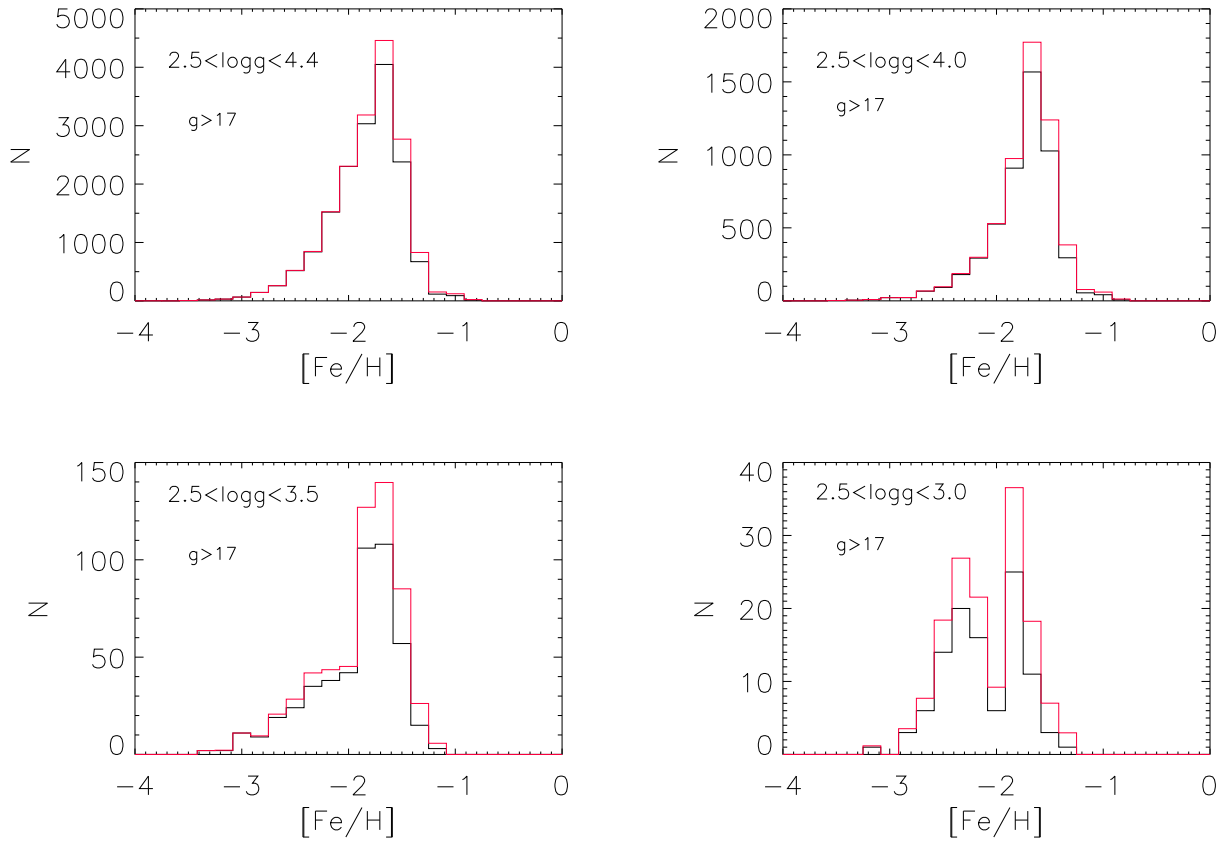

Fig. 5. Metallicity distribution derived from BOSS spectra of *spectrophotometric standard* stars. Black lines are as measured, and red lines after correcting selections effects as explained in the text. The upper two panels show the distributions for stars with two different upper limits on surface gravity, $\log g$. The two lower panels illustrate the change in metallicity distribution for stars exploring the more distant regions of the halo system.

The observed metallicity distribution is biased by to the color cuts adopted to select the BOSS spectrophotometric standard stars, i.e., Eq. 1. To evaluate this bias quantitatively, we make use of the spectral energy distributions provided with the very same Kurucz model atmospheres described in Section 3. We calculate the SDSS *ugriz* colors for stars with different atmospheric parameters, using the fiducial filter responses (Gunn 2001, private communication[5]) for a point source at an airmass of 1.3. They correspond to measurements performed in 2000, but see the discussion by Doi et al. (2010) for more details on the time stability of the SDSS filter responses. The results are given in Table 1, available in electronic format.

By selecting models in Table 1 within the temperature range $5600 \leq T_{\rm eff} \leq 6500$ K and identifying which ones would make it through the color cut in Eq. 1, we evaluate how the color selection distorts the underlying metallicity distribution. This is illustrated in Figure 4. In this figure we show 2D gray-scale maps of the distribution in $\log g$ and [Fe/H] for models within the range in temperature stated above in Table 1, before (top panel) and after applying the color selection appropriate to BOSS spectrophotometric standards (middle panel). These results were obtained using bins of 1.0 dex for both $\log g$ and [Fe/H], and interpolating linearly for an improved resolution. The bottom panel shows the ratio of the arrays depicted in the middle and top panels, i.e. the fraction of models that pass the color cut. From Figure 4 it is obvious that the color cut used to select spectrophotometric standards is very efficient at removing high-metallicity stars, and it becomes more efficient at low gravities.

The resulting metallicity distribution function is depicted in Figure 5. Each panel shows samples subjected to different magnitude and gravity cuts. The corrections associated with the color cut are fairly small. The top two panels are limited to stars with $g > 17$ and either $2.5 < \log g < 4.4$ (top-left) or $2.5 < \log g < 4$ (top-right). The more stringent gravity cut is introduced to ensure that all our stars are at least 5 kpc away, minimizing contributions from the thick disk or metal-weak thick disk. However, both distributions are very similar, indicating that the color cut is in fact very efficient at selecting halo stars. In all cases we are also limiting the samples to stars with $T_{\rm eff} > 5600$ K and $\log \chi^2 < 0.5$. For the bulk of the halo, the metallicity distribution peaks at about [Fe/H]$= -1.6$, in good agreement with previous determinations. However, there are some striking differences with earlier results that we discuss below. Table 2 provides the number of stars in each bin for the largest subsample ($g > 17$ and $2.5 < \log g < 4.4$).

The metallicity distribution published by Allende Prieto et al. (2006), based on SDSS spectra included in DR6 for G- and F-type stars located at more than 8 kpc from the plane has an extended tail toward low metallicity, similar to our results, but it extends to significantly higher metallicities. The distribution we derived is also more concentrated and asymmetric than previous

[5] http://www.sdss.org/dr3/instruments/imager/#filters

results from photometric calibrations (Ivezic et al. 2008, An et al. 2013). Our results are perhaps more similar to those by Li et al. (2010), but those authors do not separate halo and thick-disk stars at high metallicity.

The two bottom panels in Fig. 5 show the metallicity distributions for much more restricted samples, which are limited to stars with lower gravities, hence more distant, but still with $g > 17$ in both cases. For $2.5 < \log g < 3$ (bottom right panel), we limit the sample to stars beyond 10 kpc. In this panel we find a clear shift of the distributions to lower metallicities, in line with results by Carollo et al. (2007, 2010), de Jong et al. (2010), and Beers et al. (2012). The metallicity peaks at [Fe/H]$= -1.6$ and [Fe/H]$= -2.2$ resemble those associated by these authors with the inner and outer halo of the Galaxy.

5. Conclusions

We analyzed a large sample of F-type halo turnoff stellar spectra obtained by the SDSS-III BOSS project. We upgraded our analysis methods to better account for instrumental distortions and systematic calibration errors and derived the main atmospheric parameters, including the overall iron abundance.

Our results compare well with previously published analyses of SDSS spectra. The analysis of stars in the globular cluster M13 shows that the [Fe/H] estimations from this work have less dispersion than those provided up to now by the SSPP, although low-gravity metal-poor stars suffer from underestimated gravities and metallicities. Relative to previous work, we reach more distant regions of the Galactic halo with a highly homogeneous sample of F-type turnoff stars.

Our experiments indicate that selection effects associated with the color cuts used in SDSS to select these stars cause no significant distortions in the observed metallicity distributions. We find a halo metallicity distribution that peaks at around [Fe/H]$= -1.6$, in agreement with a plethora of previous studies. Nonetheless, our distribution is more sharply concentrated, with a rapid fall-off on the high-metallicity side, including very few stars at [Fe/H]> -1 and an extended tail toward very low metallicities.

The most distant stars in our sample, at tens of kpc from the Sun, hint at a significant change in the metallicity distribution, which shifts toward lower metallicities, consistent with expectations if the halo of the Milky Way comprises both an inner- and an outer-halo population. However, this has been the subject of an intense debate in the last few years (see, e.g., Beers et al. 2012 vs. Schoenrich et al. 2014) which we do not pretend to solve in this paper, since we are focused on a small fraction of the spectra obtained by the SDSS.

At this point we have only considered the overall metallicity of the stars, as derived from all metal lines available in BOSS spectra (380-920 mm). At the lowest metallicities and for the surface temperatures of the F-type stars considered, the derived metallicities are dominated by the signal in the CaII lines, whereas at higher metal abundances our metallicity determinations are dominated by large numbers of iron lines. In the following papers, we will separate individual elements and revisit the halo metallicity distribution. We will also infer distances to the stars and examine possible variations in metal abundances as a function of distance from the Galactic center in more detail.

Acknowledgements. We are grateful to Ivan Hubeny and Lars Koesterke for help with calculations of opacities and model spectra, to David Schlegel for stimulating discussions and advice, and Steph Snedden and Howard Brewington for their observations. TCB acknowledges partial support for this work by grant PHY 08-22648: Physics Frontiers Center/Joint Institute for Nuclear Astrophysics (JINA), awarded by the U.S. National Science Foundation. YSL is a Tombaugh Fellow at New Mexico State University.

Funding for SDSS-III has been provided by the Alfred P. Sloan Foundation, the Participating Institutions, the National Science Foundation, and the U.S. Department of Energy Office of Science. The SDSS-III web site is http://www.sdss3.org/.

SDSS-III is managed by the Astrophysical Research Consortium for the Participating Institutions of the SDSS-III Collaboration including the University of Arizona, the Brazilian Participation Group, Brookhaven National Laboratory, University of Cambridge, Carnegie Mellon University, University of Florida, the French Participation Group, the German Participation Group, Harvard University, the Instituto de Astrofisica de Canarias, the Michigan State/Notre Dame/JINA Participation Group, Johns Hopkins University, Lawrence Berkeley National Laboratory, Max Planck Institute for Astrophysics, Max Planck Institute for Extraterrestrial Physics, New Mexico State University, New York University, Ohio State University, Pennsylvania State University, University of Portsmouth, Princeton University, the Spanish Participation Group, University of Tokyo, University of Utah, Vanderbilt University, University of Virginia, University of Washington, and Yale University.

Table 1. Calculated *ugriz* colors for stars with different atmospheric parameters. Full table available in electronic form

[Fe/H]	$T_{\rm eff}$	$\log g$	$(u-g)_0$	$(g-r)_0$	$(r-i)_0$	$(i-z)_0$
0.5	3500	0.00	3.873	1.472	1.308	0.717
0.5	3500	0.50	3.519	1.374	1.402	0.752
0.5	3500	1.00	3.176	1.288	1.477	0.782
0.5	3500	1.50	2.845	1.215	1.533	0.805
...	...	...	...	...	...	...

Table 2. Metallicity distribution derived from BOSS spectra of spectrophotometric standards with $T_{\rm eff} > 5600$ K, $2.5 \leq \log g \leq 4.4$, and $g > 17$. All metallicity bins are 0.1 dex wide.

[Fe/H] (bin center)	N	N/Ntotal
-4.000	1	0.0001
-3.833	1	0.0001
-3.667	0	0.0000
-3.500	5	0.0003
-3.333	16	0.0009
-3.167	30	0.0017
-3.000	65	0.0038
-2.833	144	0.0084
-2.667	260	0.0151
-2.500	521	0.0302
-2.333	845	0.0490
-2.167	1525	0.0884
-2.000	2305	0.1336
-1.833	3183	0.1845
-1.667	4459	0.2584
-1.500	2768	0.1605
-1.333	828	0.0480
-1.167	152	0.0088
-1.000	121	0.0070
-0.833	21	0.0013
-0.667	0	0.0000
-0.500	0	0.0000
-0.333	0	0.0000
-0.167	0	0.0000
0.000	0	0.0000

References

Abazajian, K., Adelman-McCarthy, J. K., Agüeros, M. A., Allam, S. S., Anderson, S. F., Annis, J., Bahcall, N. A., Baldry, I. K., Bastian, S., Berlind, A., et al. 2003, AJ, 126, 2081-2086

Abazajian, K., Adelman-McCarthy, J. K., Agüeros, M. A., Allam, S. S., Anderson, S. F., Annis, J., Bahcall, N. A., Baldry, I. K., Bastian, S., Berlind, A., et al. 2004, AJ, 128, 502-512

Adelman-McCarthy, J. K., Agüeros, M. A., Allam, S. S., Allende Prieto, C. et al. 2008, ApJS, 175, 297-313
Ahn, C. P., Alexandroff, R., Allende Prieto, C., et al. 2012, ApJS, 203, 21
Ahn, C. P., Alexandroff, R., Allende Prieto, C., et al. 2014, ApJS, 211, 17
Aihara, H., Allende Prieto, C., An, D., et al. 2011, ApJS, 193, 29
Allende Prieto, C., Beers, T. C., Wilhelm, R., et al. 2006, ApJ, 636, 804
Allende Prieto, C. 2008, Physica Scripta Volume T, 133, 014014
Allende Prieto, C., Hubeny, I., & Smith, J. A. 2009, MNRAS, 396, 759
Allende Prieto, C., Lambert, D. L., Hubeny, I., & Lanz, T. 2003, ApJS, 147, 363
Allende Prieto, C., Sivarani, T., Beers, T. C., et al. 2008, AJ, 136, 2070
An, D., Beers, T. C., Johnson, J. A., et al. 2013, ApJ, 763, 65
Aoki, W., Beers, T. C., Lee, Y. S., et al. 2013, AJ, 145, 13
Asplund, M., Grevesse, N., & Sauval, A. J. 2005, Cosmic Abundances as Records of Stellar Evolution and Nucleosynthesis, 336, 25
Baade, W. 1944, ApJ, 100, 137
Barklem, P. S. 2007, Spectral Line Shapes in Astrophysics, 938, 111
Beers, T. C., Carollo, D., Ivezić, Ž., et al. 2012, ApJ, 746, 34
Beers, T. C., Preston, G. W., & Shectman, S. A. 1985, AJ, 90, 2089
Beers, T. C., Preston, G. W., & Shectman, S. A. 1992, AJ, 103, 1987
Bohlin, R. C., & Gilliland, R. L. 2004, AJ, 128, 3053
Bolton, A. S., Schlegel, D. J., Aubourg, É., et al. 2012, AJ, 144, 144
Bonifacio, P., Sbordone, L., Caffau, E., et al. 2012, A&A, 542, A87
Caffau, E., Bonifacio, P., François, P., et al. 2012, A&A, 542, A51
Carollo, D., Beers, T. C., Chiba, M., et al. 2010, ApJ, 712, 692
Carollo, D., Beers, T. C., Lee, Y. S., et al. 2007, Nature, 450, 1020
Casagrande, L., Ramírez, I., Meléndez, J., Bessell, M., & Asplund, M. 2010, A&A, 512, A54
Castelli, F., & Kurucz, R. L. 2004, arXiv:astro-ph/0405087, Proceedings of the IAU Symp. No 210; IAU Symp. No 210, Modelling of Stellar Atmospheres, eds. N. Piskunov et al. 2003, poster A20
Chamberlain, J. W., & Aller, L. H. 1951, ApJ, 114, 52
Chiba, M., & Beers, T. C. 2000, AJ, 119, 2843
Christlieb, N., Wisotzki, L., & Graßhoff, G. 2002, A&A, 391, 397
Christlieb, N., Wisotzki, L., Reimers, D., et al. 1999, The Third Stromlo Symposium: The Galactic Halo, 165, 259
Cohen, J. G., Christlieb, N., Thompson, I., et al. 2013, ApJ, 778, 56
Dawson, K. S., Schlegel, D. J., Ahn, C. P., et al. 2013, AJ, 145, 10
Dekker, H., D'Odorico, S., Kaufer, A., Delabre, B., & Kotzlowski, H. 2000, Proc. SPIE, 4008, 534
Doi, M., Tanaka, M., Fukugita, M., et al. 2010, AJ, 139, 1628
Eisenstein, D. J., Weinberg, D. H., Agol, E., et al. 2011, AJ, 142, 72
Fukugita, M., Ichikawa, T., Gunn, J. E., et al. 1996, AJ, 111, 1748
Girardi, L., Bertelli, G., Bressan, A., et al. 2002, A&A, 391, 195
Gunn, J. E., Siegmund, W. A., Mannery, E. J., et al. 2006, AJ, 131, 2332
Ivezić, Ž., Sesar, B., Jurić, M., et al. 2008, ApJ, 684, 287
de Jong, J. T. A., Yanny, B., Rix, H.-W., et al. 2010, ApJ, 714, 663
Koesterke, L. 2009, American Institute of Physics Conference Series, 1171, 73
Koesterke, L., Allende Prieto, C., & Lambert, D. L. 2008, ApJ, 680, 764
Lee, Y. S., Beers, T. C., Sivarani, T., et al. 2008, AJ, 136, 2050
Lee, Y. S., Beers, T. C., Sivarani, T., et al. 2008, AJ, 136, 2022
Lee, Y. S., Beers, T. C., Allende Prieto, C., et al. 2011, AJ, 141, 90
Li, H. N., Christlieb, N., Schörck, T., et al. 2010, A&A, 521, A10
Majewski, S. R. 1992, ApJS, 78, 87
Noguchi, K., Aoki, W., Kawanomoto, S., et al. 2002, PASJ, 54, 855
Norris, J., Bessell, M. S., & Pickles, A. J. 1985, ApJS, 58, 463
Oke, J. B. 1990, AJ, 99, 1621
Prugniel, P., & Soubiran, C. 2001, A&A, 369, 1048
Prugniel, P., Soubiran, C., Koleva, M., & Le Borgne, D. 2007, arXiv:astro-ph/0703658
Ryan, S. G., & Norris, J. E. 1991, AJ, 101, 1835
Ramírez, I., Allende Prieto, C., Redfield, S., & Lambert, D. L. 2006, A&A, 459, 613
Schlegel, D. J., Finkbeiner, D. P., & Davis, M. 1998, ApJ, 500, 525
Schönrich, R., Asplund, M., & Casagrande, L. 2014, ApJ, 786, 7
Smee, S., Gunn, J. E., Uomoto, A., et al. 2012, submitted to AJ, arXiv:1208.2233
Smolinski, J. P., Lee, Y. S., Beers, T. C., et al. 2011, AJ, 141, 89
Stoughton, C., Lupton, R. H., Bernardi, M., et al. 2002, AJ, 123, 485
Tull, R. G. 1998, Proc. SPIE, 3355, 387
Wisotzki, L., Koehler, T., Groote, D., & Reimers, D. 1996, A&AS, 115, 227
Yanny, B., Rockosi, C., Newberg, H. J., et al. 2009, AJ, 137, 4377
Yong, D., Norris, J. E., Bessell, M. S., et al. 2013, ApJ, 762, 27
York, D. G., Adelman, J., Anderson, J. E., Jr., et al. 2000, AJ, 120, 1579